Bioactive Materials 12 (2022) 107–119

Contents lists available at ScienceDirect

Bioactive Materials

journal homepage: www.keaipublishing.com/en/journals/bioactive-materials

In situ delivery of apoptotic bodies derived from mesenchymal stem cells via a hyaluronic acid hydrogel: A therapy for intrauterine adhesions

Liaobing Xin [a,c,1], Cheng Wei [a,c,1], Xiaomei Tong [a,c,1], Yangyang Dai [a,b,c], Dong Huang [a,c], Jianmin Chen [a,c], Lie Ma [b,c,**], Songying Zhang [a,c,*]

[a] Assisted Reproduction Unit, Department of Obstetrics and Gynecology, Sir Run Run Shaw Hospital, School of Medicine, Zhejiang University, Hangzhou, 310016, China
[b] MOE Key Laboratory of Macromolecular Synthesis and Functionalization, Department of Polymer Science and Engineering, Zhejiang University, Hangzhou, 310027, China
[c] Key Laboratory of Reproductive Dysfunction Management of Zhejiang Province. No. 3 Qingchun East Road, Jianggan District, Hangzhou, 310016, China

ARTICLE INFO

Keywords:
Apoptotic bodies
Mesenchymal stem cells
Endometrial regeneration
Intrauterine adhesions
Tissue engineering

ABSTRACT

Stem cell-based and stem cell-derived exosome-based therapies have shown promising potential for endometrial regeneration and the clinical treatment of intrauterine adhesions (IUAs). Evidence shows that apoptosis occurs in a majority of grafted stem cells, and apoptotic bodies (ABs) play a critical role in compensatory tissue regeneration. However, the therapeutic potential of AB-based therapy and its mechanism have not been explored in detail. Here, a cell-free therapeutic strategy was developed by incorporating mesenchymal stem cell-derived ABs into a hyaluronic acid (HA) hydrogel to achieve endometrial regeneration and fertility restoration. Specifically, we found that the ABs could induce macrophage immunomodulation, cell proliferation, and angiogenesis *in vitro*. The HA hydrogel promoted the retention of ABs and facilitated their continuous release. In a murine model of acute endometrial damage and a rat model of IUAs, *in situ* injection of the AB-laden HA hydrogel could efficiently reduce fibrosis and promote endometrial regeneration, resulting in the fertility restoration. Consequently, ABs show good potential as therapeutic vesicles, and the AB-laden HA hydrogel appears to be a clinically feasible and cell-free alternative for endometrial regeneration and IUA treatment.

1. Introduction

During women's reproductive age, 5% of women experience two or more miscarriages [1], and most of them are treated using curettage [2]. Moreover, 15–20% of patients receiving curettage develop intrauterine adhesions (IUAs) [3], and women receiving post-partum curettage show an increased risk of IUAs (21–40%) [4]. Due to severe damage to the basal layer of endometrium, IUAs are associated with infertility [5]. Traditionally, IUAs are treated using endometrial synechiotomy, intrauterine devices, and estrogen therapy [5]. However, the re-construction of functional endometrium in moderate and severe cases remains a major challenge. Moreover, the rate of IUA recurrence in moderate and severe cases is high (33.3%–45.7%) [6–8], whereas the rate of pregnancy is low (23.7%–27.7%) [8–10].

Over the last decade, cell therapies involving the implantation of stem cells derived from different sources to regenerate the endometrium have been considered the most promising strategy for IUAs [11–13]. Among them, human umbilical cord-derived mesenchymal stem cells (huMSCs) offer regenerative benefits via the secretion of paracrine factors [14,15]. The safety and therapeutic effects of huMSCs have been confirmed in patients with mild–moderate IUAs [11]. However, under clinical conditions, there are several limitations to cell therapies, including immunogenicity, uncontrolled cell differentiation and tumorigenic risk [16]. In recent years, stem cells derived exosomes have been proved to have the ability to modify the function of recipient cells and have low immunogenicity, making them an excellent alternative to

Peer review under responsibility of KeAi Communications Co., Ltd.
* Corresponding author. Assisted Reproduction Unit, Department of Obstetrics and Gynecology, Sir Run Run Shaw Hospital, School of Medicine, Zhejiang University; Hangzhou, 310016, China.
** Corresponding author. MOE Key Laboratory of Macromolecular Synthesis and Functionalization, Department of Polymer Science and Engineering, Zhejiang University, Hangzhou, 310027, China.
E-mail addresses: liema@zju.edu.cn (L. Ma), zhangsongying@zju.edu.cn (S. Zhang).
[1] These authors contributed equally to this work.

https://doi.org/10.1016/j.bioactmat.2021.10.025
Received 12 July 2021; Received in revised form 30 September 2021; Accepted 17 October 2021
Available online 22 October 2021

living cell-based therapies for tissue regeneration [17–20].

Notably, MSCs undergo apoptosis and release apoptotic bodies (ABs) during cell therapy. ABs contain multiple functional biomolecules, including microRNAs, mRNA, DNA, lipids, and proteins [21]. They can diffuse within tissues and trigger compensatory proliferation in surrounding cells and maintain tissue homeostasis after wounding [22,23]. ABs are also associated with immune modulation [24]. In the field of regenerative medicine, ABs have been found to ameliorate osteopenia, promote bone defect healing and cutaneous wound healing [25–27]. However, the therapeutic potential of AB in cases of IUAs and the mechanism of their action have not been explored yet.

Recently, to increase the retention and engraftment of stem cells and their derivatives for endometrial regeneration, multiple scaffold materials that act as delivery systems have been fabricated [28–30]. In our previous study, huMSC and huMSC-derived exosomes were decorated in a collagen scaffold (CS), and the implantation of these compound scaffolds successfully induced endometrial regeneration and restored fertility [31,32]. Akin to cells and exosomes, the low retention and engraftment abilities of ABs also influence their delivery efficiency. However, CS cannot adapt to the irregular shape of the uterine cavity, and the implantation procedure of CS is more complex than the procedure of minimally invasive injection of hydrogel. Therefore, a hyaluronic acid (HA) hydrogel, showing good biocompatibility, biofunctionality, biodegradability and injectability, has been adopted as a matrix for ABs [33,34]. Moreover, HA hydrogel has been successfully applied to prevent postoperative IUAs in clinic [2,35]. Here, an AB-laden HA hydrogel was fabricated, and its therapeutic effect and mechanism of action were investigated. As shown in Fig. 1a, ABs secreted from apoptotic huMSCs were mixed with the HA hydrogel to yield an AB-laden HA hydrogel to achieve cell-free endometrial regeneration *in situ*. In this mixture, the HA hydrogel would offer a mechanical barrier for wounded area isolation and the incorporated ABs would offer

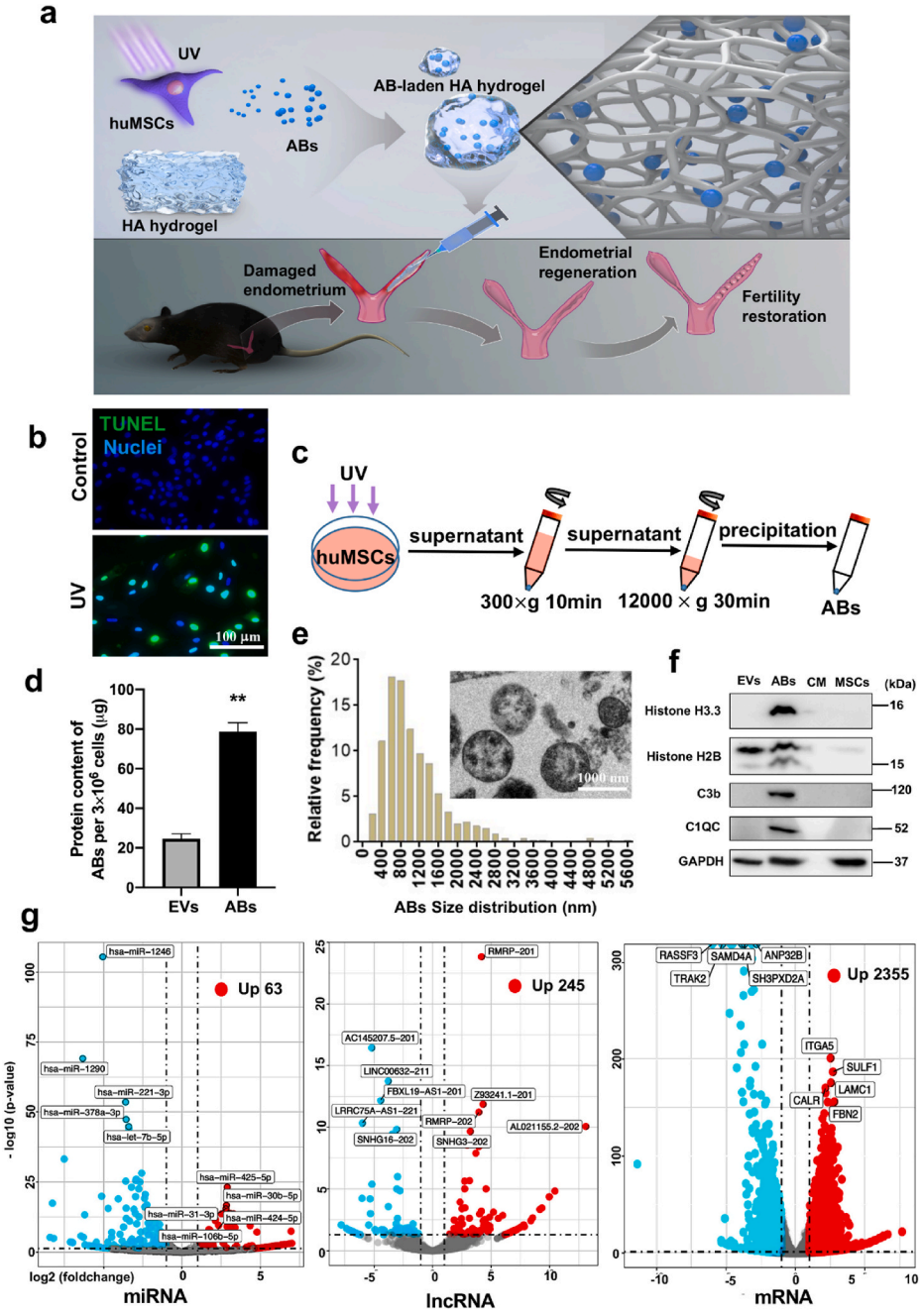

Fig. 1. Schematic illustration of the design and application of the apoptotic body (AB)-laden hyaluronic acid (HA) hydrogel, and the characterization of ABs derived from human umbilical cord-derived mesenchymal stem cells (huMSCs). (Print in colour) a) Schematic illustration of the design and application of the AB-laden HA hydrogel, which consisted of ABs production from apoptotic huMSCs for administration into the uterine cavity via a hyaluronic acid (HA) hydrogel *in situ* to promote endometrial regeneration and fertility restoration. b) Confocal images of the TUNEL-stained (green) huMSCs with UV treatment, those cells with no UV treatment served as the control, and all cells were labelled with DAPI (blue). c) Schematic of the procedure used for the isolation procedure of ABs via differential centrifugation. d) Relative protein content in ABs secreted from UV-treated huMSCs and extracellular vesicles (EVs) from no-UV-treated huMSCs. Data were normalized to the number of huMSCs in each plate (n = 7). e) Size distribution of ABs measured from transmission electron micrographs (TEM). Inset is a typical TEM image of ABs. f) Western blot analysis of ABs for H3.3, H2B, C1QC, C3b, and β-actin. g) Volcano plot showing significantly upregulated (red dots) and downregulated (blue dots) miRNAs, lncRNAs and mRNAs in ABs, compared to EVs. **p < 0.01.

biochemical cues. We investigated the effects of ABs on macrophage immunomodulation, cell proliferation, and vascular formation *in vitro*. Then, we tested the therapeutic effects of the AB-laden HA hydrogel on endometrial regeneration, collagen remodeling, endometrial receptivity, and fertility restoration in a murine model of acute endometrial damage and a rat model of IUA. Further, we explored the potential therapeutic mechanism of the AB-laden HA hydrogel *in vivo*.

2. Materials and methods

2.1. Cell culture, AB isolation, and AB identification

huMSCs were obtained from Boyalife Group Ltd. (HTX2318, Wuxi, China). The identification of huMSCs and their multipotent differentiation potential had been investigated previously [31]. Cells having undergone fewer than six passages were maintained in Dulbecco's modified Eagle medium/F-12 (DMEM/F-12, Gino Biological, Hangzhou, China) with 10% (*v/v*) fetal bovine serum (FBS, SA112.02, Cellmax, Beijing, China). The confluent monolayers of huMSCs kept in uncovered Petri dishes were exposed to UVC light (30W, 254 nm, Philip, China) for 25 min at an intensity of 600 mJ/cm^2 [24]. Apoptosis in huMSCs was evaluated using a terminal deoxynucleotidyl transferase (TdT)-mediated dUTP nick end labeling (TUNEL) assay (MA 0223, Meilunbio, China) according to the manufacturer's protocol, and the apoptotic cells were observed using a confocal microscope (Olympus FV3000, Japan).

After 24-h culture of UV-treated huMSCs, culture medium was collected (10 mL per 3 × 10^6 cells) and precleared by 300×*g* for 10 min at 4 °C. Then, the supernatant was collected and further centrifuged at 12000×*g* for 30 min. The pellet was washed with phosphate-buffered saline (PBS), recentrifuged, and suspended in PBS (40 μL per 3 × 10^6 cells, 1200 μg/mL in PBS). The purified ABs were quantified using the BCA protein assay kit (Thermo Fisher Scientific, USA). ABs were characterized by transmission electron microscopy (TEM) (Tecnai T10, Philips, Netherlands) and western blot analysis for specific AB markers (see supplemental Methods for details). Component analysis of ABs were performed using RNA sequencing (RNA-seq) analysis (see supplemental Methods for details). The extracellular vesicles (EVs) isolated from the culture medium of non-UV-treated huMSCs using the same isolation procedure as ABs were used as control.

For *in vitro* experiments, ABs was resuspended in fresh culture medium at 24 μg/mL concentration (diluted in culture medium), which was 5-fold correspond to supernatant of UV-treated huMSCs. This concentration was considered relevant as the concentration of MSC-derived condition medium in our previous research on endometrial stromal cells was shown to be 5-fold correspond to supernatant [36]. For *in vivo* experiments, 24 μg of ABs (20 μL, 1200 μg/mL, derived from 1.5 × 10^6 cells) was injected in the murine model and 96 μg of ABs (80 μL, 1200 μg/mL, derived from 6 × 10^6 cells) was injected in the rat model. This concentration was considered relevant as the amount of MSCs transplanted in mice IUA model and rat IUA model was shown to be in the range of (0.5–2) × 10^6 [37,38]and (3-10) × 10^6 [39,40].

2.2. Examination of AB-induced macrophage immunomodulation

The endometrial regeneration process in menstrual physiology is analogous to that in classic wound healing, including inflammation, its resolution, angiogenesis, tissue formation and remodeling. In the process, multiple of cells participate and exert function synergistically. Here we examined the ABs effect on macrophages, human endometrial stromal cells (HESCs), Ishikawa cells (human endometrial carcinoma cell line, as the replacement for endometrial epithelial cells) and human vein endothelial cells (HVECs), which are commonly involved in endometrial repair.

Detailed methodology on isolation of macrophages can be found in supplemental Methods. Macrophages were cultivated for 24 h, then were seeded in 6-well plates with a concentration of 1.3 × 10^6/cm^2 and incubated in 2 mL RPMI-1640 containing 10% FBS and 24 μg/mL ABs for 24 h, with or without subsequent lipopolysaccharide (LPS) (InvivoGen, USA) (100 ng/mL) addition (incubation, 2 h). Macrophages with no added ABs, irrespective of LPS stimulation, served as the control. Macrophage phenotypes were determined using immunofluorescence staining, and specific genes associated with immunomodulation were analyzed using quantitative real-time polymerase chain reaction (qRT-PCR) (see supplemental Methods for details). All primers are listed in Table S1.

2.3. Examination of AB-induced cell proliferation, migration and fibrotic gene expression

Detailed methodology on isolation of HESCs can be found in supplemental Methods. HESCs were seeded in 96-well plates (2 × 10^3 cells per well) and incubated in DMEM/F-12 containing 10% FBS and 24 μg/ml ABs. Ishikawa cells were purchased from Procell Ltd. (RL95-2, Wuhan, China) and cultured in DMEM/F12 plus 10% FBS in 96-well plates (1 × 10^3 cells per well). The proliferative behaviors of HESCs and Ishikawa cells were evaluated using a cell counting kit-8 (CCK-8) assay (Dojindo, Shanghai, China) according to the manufacturer's protocol. Cells cultured by DMEM/F-12 with 10% FBS served as controls.

To evaluate the effect of ABs on migration of HESCs, cells were seeded into 6-well plates (3 × 10^5 cells per well) and cultured in DMEM/F-12 containing 10% FBS until confluent monolayers. A linear wound was made using a 200 μL pipette tip. After washed with PBS, cells were incubated in DMEM/F-12 containing 10% FBS and 24 μg/ml ABs. The area of the scratch was measured at 0 h, 6 h and 24 h through taking six representative images. The closure rate was calculated as follows:

$$\text{Closure percent } \% = 100 - \text{scratch area at 6 h or 24 h / scratch area at 0 h} \times 100.$$

To evaluate the effect of ABs on fibrotic gene expression of HESCs, qRT-PCR on fibrotic genes (*Col IA2*, *Fibronectin [FN], connective tissue growth factor [CTGF],* and *α-SMA*) was performed, all primers are listed in Table S1, and data were normalized using β-actin expression (see supplemental Methods for details).

2.4. Examination of AB-induced angiogenesis

A tube formation assay was performed. HUVECs were purchased from Procell Ltd. (HTX2104, Wuhan, China). Diluted Matrigel (BD Biosciences, USA, 5 mg/mL, 100 μL) was added to 48-well plates and then left to harden. A HUVEC suspension (2 × 10^5 cells/mL, 200 μL) diluted with DMEM/F-12 containing 10% FBS was added and incubated for 1 h to allow cells to adhere. Then, 200 μL ABs (24 μg/mL, diluted in DMEM/F-12 containing 10% FBS) was added to each well, and the cells were incubated for 2 h at 37 °C. Following this, the presence of capillary-like structures was examined using a digital light microscope (Leica, Germany).

2.5. Examination of AB-induced increase in mitochondrial bioenergetics

For measuring the total adenosine 5′-triphosphate (ATP) production, macrophages were seeded in 24-well plates at a density of 200,000 cells per well and incubated with 500 μL ABs (24 μg/mL in RPMI-1640 containing 10% FBS) for 24 h. Subsequently, the ATP in the cell lysate of each well was measured using an Enhanced ATP Assay Kit (Beyotime, China) according to the manufacturer's protocol. Cells in medium not containing ABs were used as controls.

To evaluate the effect of ABs on mitochondrial bioenergetics in macrophages, HESCs, and HUVECs, oxygen consumption rates (OCR) was measured using a Seahorse XFp Extracellular Flux Analyzer (Agilent Technologies, USA). Macrophages, HESCs, and HUVECs were seeded on customized Seahorse 8-well cartridges at densities of 40,000, 25,000, and 25,000 cells/well, respectively; then all cells were incubated with

80 μL ABs (24 μg/mL, diluted in culture medium) for 24 h. Cells cultured by medium not containing ABs were used as controls. All cells were incubated in XF assay media for 1 h at 37 °C. Meanwhile, specific inhibitors (oligomycin, carbonyl cyanide 4-trifluoromethoxy phenylhydrazone [FCCP], and rotenone/antimycin A) were prepared according to manufacturer instructions. Cartridges containing cells with inhibitor-containing probe cartridges were placed in the machine, and the Mito Stress Test was performed. In this process, three inhibitors were injected into the cell solution sequentially. OCR readouts were produced, and all values were normalized based on the cell number in each well.

2.6. Construction and characterization of the AB-laden HA hydrogel

The AB-laden HA hydrogel was prepared by incubating 50 μL of AB solution (2400 μg/mL in PBS) with 50 μL HA (5 mg/mL, Bioregen, China) overnight at 4 °C. The self-cross-linking HA had been approved by the China Food & Drug Administration as a physical barrier for clinical administration (no. 20153641542). To confirm the incorporation of ABs with HA hydrogel, the composite hydrogel was assessed using scanning electron microscopy (SEM) (HITACHI S–3000 N, Japan); Dil-labelled AB-laden HA was fabricated and assessed by confocal laser scanning microscopy (CLSM) (Olympus FV3000, Japan). The release profile of ABs from the composite hydrogel submerged in hyaluronidase (50 ng/mL, diluted in PBS) at 37 °C was examined. Briefly, the 100 μL HA hydrogel containing 120 μg ABs was placed in the upper transwell chamber with 0.4-μm pore (Corning, NY) and 200 μL hyaluronidase was added into the lower chamber. 100 μL leaching solution was collected and replaced by 100 μL hyaluronidase at time points 4 h, 12 h, 24 h, 36 h, 48 h, 72 h, 96 h and 120 h until the sample had degraded. The protein content of released ABs was detected by the BCA protein assay kit (Thermo Fisher Scientific, USA). The release efficiency of ABs was calculated as follows:

AB release efficiency % = cumulative protein content of ABs in the leaching solution / total protein content of ABs loaded onto HA × 100%.

2.7. In vivo evaluation of the degradation of the AB-laden HA hydrogel and fluorescence imaging analysis of Dil-labelled AB-laden HA hydrogel in uteri

The *in vivo* studies were approved by the Institutional Animal Care and Use Committee of the Zhejiang Academy of Medical Sciences (SRRSH20200103) and followed the National Institutes of Health guidelines for animal care (NIH Publications No. 8023, revised 1978). Female C57BL/6 mice (20 g, 8 weeks old) and Female Sprague-Dawley (SD) rats (230 g, 8–9 weeks) were housed in a well-controlled environment with a regulated light/dark cycle (12/12 h, 22 °C–26 °C). A total of 140 mice and 98 rats were used in the experiment. After 7 days of acclimatization, all mice underwent vaginal smear examination to ensure cycle synchronization. After surgery, meloxicam (5 mg/kg) was administered every 12 h for 3 times and at the experimental endpoint, euthanasia was administered using an overdose of anesthetic.

The degradation of AB-laden HA hydrogel *in vivo* were evaluated in rat and 20 uterine horns (4 uterine horns at each time point) were used. After anesthesia, the uterine horns were exposed and received an injection of the AB-laden HA hydrogel (80 μL) after endometrial scraping. Rats were sacrificed at days 1, 2, 3, 4 and 5 post-surgery, then the uteri were exposed and the retrievable hydrogel and the intrauterine liquid were collected. The uteri were thoroughly washed with 0.5 mL of PBS and collected. The remnant of the HA in the collected PBS and liquid from uterine cavity was measured using a Hyaluronan Quantification Kit (EU2556, Enfei, China). Insoluble HA was subjected to hyaluronidase (200 μg/mL in PBS) treatment and its concentration was measured using the same kit. The intrauterine HA remnant (%) was calculated from the weight before intrauterine implantation and the measured weight at collection.

The fluorescence tracing after Dil-labelled AB-laden HA injection was evaluated *in vivo* and a total of 15 mice (3 mice at each time point) was used. The right uterine horns were left intact and the left uterine horns received endometrial damage and Dil-labelled AB-laden HA implantation. Mice were sacrificed at days 1, 2, 5, 8 and 12 post-surgery and uteri were harvested. All samples were imaged at 583 nm emission and 556 nm excitation by an *in vivo* living imaging system (IVIS Spectrum, Perkins Elmer, American) and analyzed using the live imaging software version 4.3 (Perkins Elmer, America). Fluorescence signals of the left uterine horns were measured as total radiant efficiency, and were normalized by the background signal in the right uterine horns [41].

2.8. In vivo evaluation of the effect of the AB-laden HA hydrogel in the murine endometrial acute damage model

Detailed methodology on establish and identificate the murine acute endometrial damage model [42] can be found in supplemental Methods. Mice were divided randomly into two equal clusters. In one cluster, the left uterine horn of each mouse received no treatment after repeated endometrial scraping (natural repair group [NR group]); meanwhile, the right uterine horn of each mouse received an injection of an AB solution (20 μL, 1200 mg/mL in PBS) into the uterine cavity after repeated endometrial scraping (ABs group). In the other cluster, the left uterine horn of each mouse received an injection of HA (20 μL, diluted in PBS at a proportion of 1:1) into the uterine cavity after repeated endometrial scraping (HA group); meanwhile, the right uterine horn of each mouse received an injection of the AB-laden HA hydrogel (20 μL, containing 24 μg ABs) into the uterine cavity after repeated endometrial scraping (HA/ABs group). After surgery was completed, mice were observed for 30 min until they could move. For *in vivo* evaluation of the mechanism of action of the AB-laden HA hydrogel, some mice were euthanized 3 d and 7 d after surgery and samples were analyzed by immunofluorescent staining and enzyme-linked immunosorbent assay (ELISA). 8 uterine horns were used in each group at each time point. For endometrial regeneration and collagen remodeling assessment, some mice were euthanized 12 d after surgery and samples were analyzed by H&E and Masson's trichrome stains. 6 uterine horns were used in each group. For endometrial receptivity evaluation, some mice were mated at 12 d post-surgery and euthanized at gestational day (GD) 4 (the day a vaginal plug was observed was considered GD 1). 6 uterine horns were used in each group and an immunohistochemistry assay was performed using uterine cryosections from the uterine horns at GD 4. For fertility restoration evaluation, the groups were as follows: (i) NR group, 31 uterine horns; (ii) ABs group, 31 uterine horns; (iii) HA group, 33 uterine horns; (iv) HA/ABs group, 33 uterine horns. Mice were euthanized at GD 6–19 and the number of uterine horns with growing embryos and the number of growing embryos per uterine horn were counted. Meanwhile, the morphology of uterine horns with embryos in the HA/ABs group at GD 6, 7, 8, 10, 12, and 19 was observed, and the placenta at GD 19 were examined using H&E staining.

2.9. In vivo evaluation of the effect of the AB-laden HA hydrogel in a rat IUA model

Detailed methodology on establish and identificate the rat IUA model can be found in supplemental Methods. Established IUA rats were divided randomly into two equal clusters. Rats were treated via synechiae division using a 21-Gauge needle. Briefly, a needle was inserted into the uterine horn, rotated, and withdrawn four times to separate fibrosis adhesions and drain the effusion in the uterine cavity. In one cluster, the left uterine horn of each rat received no treatment following synechiae division (NR group), and meanwhile, the right uterine horn of

each rat received an injection of AB solution (80 μL, 1200 mg/mL in PBS) into the uterine cavity following synechiae division (ABs group). In the other cluster, the left uterine horn of each rat received an injection of HA (80 μL, diluted in PBS at 1:1 ratio) into the uterine cavity following synechiae division (HA group), and meanwhile, the right uterine horn of each rat received an injection of the AB-laden HA hydrogel (80 μL, containing 96 μg ABs) into the uterine cavity following synechiae division (HA/ABs group). To evaluate the effect of the AB-laden HA hydrogel on endometrial regeneration, some rats were euthanized 30 d and 60 d after surgery and samples were analyzed by H&E and Masson's trichrome staining. 5 uterine horns were used in each group at each time point. To evaluate the effect of the AB-laden HA hydrogel on fertility restoration, some rats were euthanized at GD 14–16 and the number of uterine horns with growing embryos and the number of growing embryos per uterine horn were counted. The groups were as follows: (i) NR group, 33 uterine horns; (ii) ABs group, 33 uterine horns; (iii) HA group, 29 uterine horns; (iv) HA/ABs group, 29 uterine horns.

2.10. Staining methods and Elisa

Detailed methodology on H&E staining, Masson's trichrome staining, immunofluorescent staining and Elisa can be found in supplemental Methods.

2.11. Statistical analysis

Continuous variables, except for those represented in violin plots, were presented as mean ± standard error of mean. Comparisons between groups with normal distribution were performed using one-way analysis of variance (ANOVA) with Tukey's multiple comparisons test or a two-tailed student's t-test. Comparisons between groups with non-normal distribution were performed using a Kruskal–Wallis test. Categorical variables were assessed using a Chi-square test. All cell quantifications and size- and fluorescence intensity-related analyses were performed using ImageJ software (National Institute of Health, USA). Differences were considered significant at p values < 0.05.

3. Results

3.1. Identification and characterizations of the ABs derived from huMSCs

UV irradiation was used to induce apoptosis in huMSCs and apoptosis appeared to be significantly higher in UV-treated huMSCs than in no-UV-treated huMSCs (control), and approximately 93.4% of the cells were apoptotic (Fig. 1b). Apoptotic blebs and vacuolar change were observed in UV-treated cells (Figs. S1a and b), compared with control. ABs were purified via sequential centrifugation (Fig. 1c). The protein content from ABs was significantly higher than EVs (Fig. 1d), indicating that UV treatment increased AB production. The ABs were spherical with a diameter of 200–3000 nm and they contained irregularly condensed cell materials (Fig. 1e). The AB expressed the AB-specific markers including histone H3.3, histone H2B, C3b, and C1QC (Fig. 1f) [31].

A total of 454 miRNAs, 380 lncRNAs and 4063 mRNAs were differentially expressed, and 63 miRNAs, 245 lncRNAs and 2355 mRNAs were upregulated significantly in ABs (Fig. 1g). Based on Gene ontology (GO) database, all the differentially expressed genes (DEGs) were included into multiple terms within the three domains 'Biological process', 'Cellular component' and 'Molecular function', indicating load of various active molecular in ABs (Figs. S2a, b, c). Based on Kyoto Encyclopedia of Genes and Genomes (KEGG) database, results of miRNAs showed that these DEGs were associated with 'Endocytosis' and 'Signaling pathways regulating pluripotency of stem cells' within the 'Cellular process' domain, 'Protein processing in endoplasmic reticulum' within the 'Genetic information processing' domain, 'Biosynthesis of amino acids' in the 'Metabolism' domain and 'Protein digestion and absorption' in the 'Organismal system' domain (Fig. S2d). Both results from lncRNAs and mRNAs analysis showed that DEGs were associated with signaling transduction, cellular behavior, as well as regulation of metabolism, such as 'Regulation of actin cytoskeleton','Endocytosis', 'protein processing in endoplasm reticulum' and 'Oxidative phosphorylation' (Figs. S2e and f).

3.2. ABs induce macrophage immunomodulation, cell proliferation, and angiogenesis in vitro

CM-Dil label was observed in macrophages pretreated with CM-Dil labelled ABs, demonstrating AB uptake by macrophages (Fig. S3a). CD163 (marker of an anti-inflammatory and pro-healing phenotype) was more frequently expressed in AB-primed macrophages than in primary macrophages, although there was no significant difference in the expression of CD86 (marker of a pro-inflammatory phenotype) (Fig. 2a). ABs significantly suppressed the activation of proinflammatory genes (*IL-1β*, *TNFα*, *IL-6*, and *IFN-γ*), while simultaneously enhancing the expression of some markers of the neovascularization response in primary macrophages (*VEGFA* and *IGF1*) (Fig. 2b). Moreover, even in LPS-stimulated macrophages, ABs significantly induced the expression of CD163 and triggered the expression of immunomodulatory and neovascularization genes (*IL-10*, *VEGFA*, *IGF1*, and *TGFβ*) (Figs. S3b, c, d).

The proliferation, migration and fibrotic genes expression of HESCs (vimentin as the specific marker, Fig. S3e) upon AB treatment were investigated. For proliferation, AB treatment significantly promoted HESCs proliferation after 3 days of co-culture (Fig. 2d). In order to investigate which range of ABs in diameter engulfed by cells, ABs larger than 1 μm (termed as ABs $^{>1\mu m}$) and those smaller than1 μm (termed as ABs $^{<1\mu m}$) were separated using a 1 μm filter (Fig. S3f). A CCK8 assay was performed to investigate the ABs $^{>1\mu m}$ and ABs $^{<1\mu m}$ on HESCs proliferation. Surprisingly, both ABs $^{>1\mu m}$ and ABs $^{<1\mu m}$ could promote HESCs proliferation significantly, compared to control group and there was no difference between ABs $^{>1\mu m}$ and ABs $^{<1\mu m}$ (Fig. S3g). The result indicated that both ABs $^{>1\mu m}$ and ABs $^{<1\mu m}$ could be engulfed and exert biological function. In addition, ABs also enhanced proliferation of Ishikawa cells from 1 to 3 days (Fig. S3h). However, there were no significant difference between ABs and control group at day 4 and 5 timepoint (Fig. S3i). As an epithelium cell line derived from endometrial carcinoma, the Ishikawa cells proliferate rapidly and should be greatly affected by contact inhibition with the prolongation of culture time. For HESCs migration, the higher closure percentage was obtained when AB was administrated, compared with control group by wound scratch assay (Fig. 2c). For fibrotic genes expression, ABs significantly suppressed the expression of fibrotic genes (*Col IA2*, *Fibronectin [FN], connective tissue growth factor [CTGF],* and *α-SMA*) (Fig. 2e).

HUVECs exhibited more intensive and extended tubular networks after co-culture with ABs (Fig. 2f). The number and total area of tubes in the ABs group were significantly higher than those in the control group (Fig. 2f). The cumulative length of tubes in the ABs group (17115 ± 565.6 μm) was also higher than that in the control group (12146 ± 392.5 μm) significantly. These result indicated that tubular network formation of HUVECs was promoted by AB treatment significantly.

3.3. ABs induce increase in mitochondrial bioenergetics

The total ATP production in macrophages was enhanced after AB co-culture (Fig. S3h). Co-culture of ABs with macrophages, HESCs, and HUVECs increased basal OCRs in these cells (Fig. 2g). Then, the cells were treated with oligomycin A, an ATP synthase inhibitor, to distinguish between ATP-linked respiration and proton leak. The levels of proton leak were higher in macrophages, HESCs, and HUVECs that were co-cultured with ABs than in those that were not (Fig. 2g). Cells were also treated with FCCP, an uncoupling agent, to observe the cell response to an increase in ATP demand. All three cell types exhibited increased OCRs following FCCP treatment, and the OCRs in all three cell

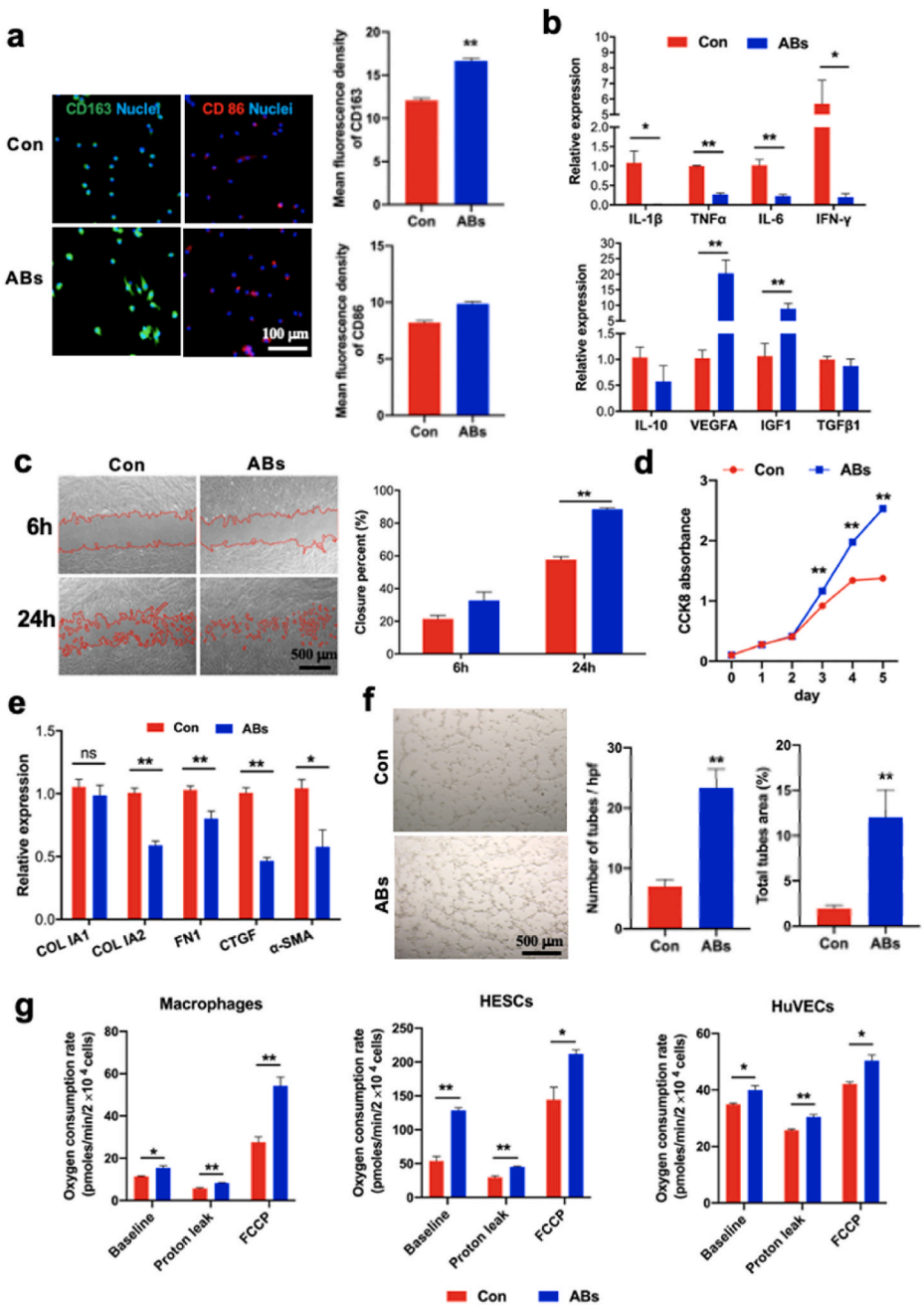

Fig. 2. Effects of ABs on macrophage phenotype, cell proliferation and angiogenesis *in vitro*. (Print in colour) a) Immunostaining for CD163 (green) and CD86 (red) in macrophages after 24 h of incubation with ABs, and mean fluorescence intensity for CD163 and CD86 (n = 15). Macrophages that were not incubated with ABs served as controls. All cells were labelled with DAPI (blue). b) Relative mRNA levels of proinflammatory genes (*IL-1β*, *TNFα*, *IL-6*, and *IFN-γ*) and pro-healing genes (*IL-10*, *VEGFA*, *IGF1*, and *TGF-β*) in macrophages cultured with ABs (n = 3). c) Representative images of scratch assay examining the migration ability of human endometrial stromal cells (HESCs) cultured with ABs and quantification of closure area (n = 6). d) Results of the cell counting kit-8 (CCK-8) assay performed for examining the proliferation of HESCs cultured with ABs for different time (n = 4). e) Relative mRNA levels of fibrotic genes (*Col IA2*, *Fibronectin [FN]*, *connective tissue growth factor [CTGF]*, and *α-SMA*) in HESCs after 24 h of incubation with ABs (n = 5). f) Representative images from the tube formation assay used to examine human umbilical vein endothelial cells (HUVECs) cultured with ABs and quantitative evaluation of the number of tubes and total tube area (n = 6). g) Oxygen consumption rates of macrophages, HESCs, and HUVECs cultured with ABs for 24 h (n = 3). All values were normalized based on the cell number in each well. *p < 0.05 and **p < 0.01.

types co-cultured with ABs were significantly higher than those in cells that were not co-cultured with ABs (Fig. 2g).

Notably, there was a significantly enrichment of DEGs of lncRNAs linked to mitochondrial bioenergetics based on GO database, including 'organelle organization', 'mitochondrion organization' 'mitochondrial respiratory chain complex I assembly' and 'NADH dehydrogenase complex assembly' in the category of 'Biological process' (Fig. S4a), 'ATP binding' and 'NADH dehydrogenase activity (ubiquinone and quinone)' in the category of 'Molecular function' (Fig. S4b), 'mitochondrial inner membrane', 'mitochondrial envelop', 'respiratory chain' and 'mitochondrial respiratory chain complex I' in the category of 'Cellular component' (Fig. S4c). Further enrichment analysis showed that 'Oxidative phosphorylation' pathway was enriched for these DEGs (Fig. S4d). The result indicate lncRNA in ABs might give the remarkable effects through the activation of mitochondrial bioenergetics.

3.4. Characterization of the AB-laden HA hydrogel

We studied the *in vitro* HA hydrogel dissolution kinetics at 37 °C in the presence of hyaluronidase, a ubiquitous enzyme for HA *in vivo* degradation (Fig. S5a). Sample 1 (dilution rate, 2:10) was dissolved at 5 h. At day 3, sample 2 (dilution rate, 5:10) partially dissolved and sample 3 (dilution rate, 8:10) was not dissolved. At day 5, sample 2 presented no more gel and sample 3 partially dissolved. The AB entrapment efficiency in HA hydrogel is 89.2 ± 0.9% (n = 3). An even distribution of CM-Dil-labelled ABs within the hydrogel matrix was observed by CLSM analysis (Fig. 3a). HA hydrogel with and without ABs exhibited porous structures by SEM analysis (Fig. 3b, and Fig. S5b), and the ABs were found to be embedded into the inner pore of HA hydrogel (Fig. 3b). A continuously release profile of ABs from the AB-laden HA hydrogel was observed and the cumulative release ratio was approximately 95% after 5 days *in vitro* in the presence of hyaluronidase (Fig. 3c). The degradation of AB-laden

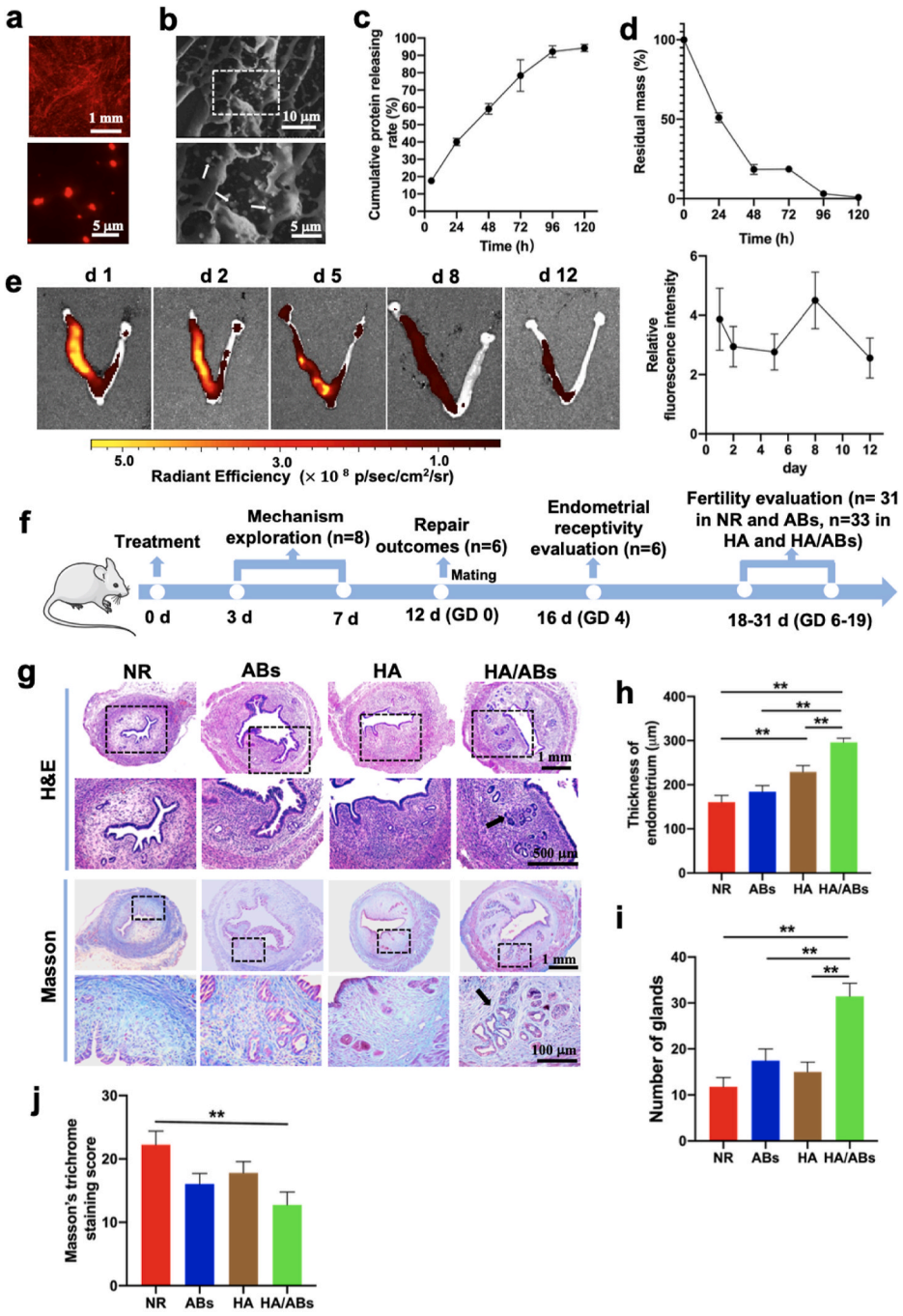

Fig. 3. Characterization of the AB-laden HA hydrogel and its effects on endometrial regeneration and collagen remodeling in a murine acute endometrium damage model. (Print in colour) a) Confocal laser scanning microscopy (CLSM) images showing the distribution of CM-Dil-labelled ABs in the AB-laden HA hydrogel. b) Scanning electron microscopy (SEM) images of the AB-laden HA hydrogel. The inset shows the region with dashed boxes at a higher magnification, and the ABs in the composite hydrogels are indicated by white arrows. c) The cumulative protein releasing profile of ABs from the AB-laden HA hydrogel in the presence of hyaluronidase (n = 3). d) Degradation of the AB-laden HA hydrogel *in vivo*. e) Representative fluorescence images of uteri at different time post-surgery by *in vivo* imaging system and quantification of fluorescent signals in uteri (n = 3). The left uterine horn of each uterus were scraped and injected with Dil-labelled AB-laden HA hydrogel. The right uterine horn were left intact. Quantification of fluorescent signals in the left uterine horns were normalized by the signals in the right uterine horns. f) Schematic of the *in vivo* study in a murine acute endometrial damage model. g) Representative images of uteri under different treatments for 12 d, examined using hematoxylin and eosin (H&E) staining and Masson's trichrome staining. The insets outlined by black dashed boxes are shown in the lower row at a higher magnification. Quantification of endometrial thickness (h) (n = 11) and endometrial glands (i) (n = 11) in (g). j) Masson's trichrome staining scores for uteri under different treatments for 12 d (n = 11). **p < 0.01.

HA *in vivo* was evaluated (Fig. 2d). At day 1, the hydrogel was observed in uterine cavity and the remnant of the AB-laden HA was 50.8%. At day 2, viscous liquid was observed and the intrauterine remnant of the AB-laden HA was 18.6%. At day 3, 4, and 5, HA-derived viscous liquid was not observed and the mean intrauterine remnant was 18.4%, 3.0% and 0.7% correspondingly. We evaluated the AB retention *in vivo* after AB-laden HA implantation by *in vivo* imaging system. Our result showed that the signals from Dil-labelled ABs in uteri persisted at robust levels until day 12 (Fig. 3e), which indicated that the retained ABs could exert continuous therapeutic function.

3.5. Cell-free AB-laden HA hydrogel induces endometrial regeneration in a murine endometrial acute damage model

A murine endometrial damage model was established as previously described [42]. Thinner endometrium, fewer endometrial glands, and more severe fibrosis were observed than normal endometrium 12 days after endometrial damage (Figs. S6a–d). As the schematic shown in Fig. 3f, the potential mechanism of the AB-laden HA hydrogel was explored at 3 and 7 d post-surgery; repair outcomes were evaluated at 12 d post-surgery; endometrial receptivity was evaluated at GD 4 and fertility restoration was evaluated at GD 6–19. There was no significant difference in the appearance of uteri following different treatments (Fig. S6e). However, the HA/ABs group exhibited a significantly thicker endometrium and a greater formation of endometrial glands (black arrows in Fig. 3g) than the NR, ABs, and HA groups (Fig. 3h and i). The light green color (collagen ingredient) was found to cover a significantly lower area in the HA/ABs groups than in the NR group (Fig. 3g, j), suggesting that less fibrosis occurred after AB-laden HA hydrogel injection.

3.6. Cell-free AB-laden HA hydrogel increases endometrial receptivity in the murine endometrium-wounded model

Establishment of pregnancy is a crucial event, and failure of embryo implantation often results in miscarriage. In mice, the endometrium becomes receptive to blastocyst implantation on GD 4 but is non-receptive on GD 5. The epithelium includes glandular epithelium (GE) and luminal epithelium (LE) and plays a critical role in successful implantation [43]. Treatment with the AB-laden HA hydrogel increased pan-cytokeratin (Pan-CK, a pan marker of epithelium) expression significantly, compared with NR, ABs alone, and HA alone treatments (Fig. 4a and b). Evidence shows that Forkhead box a2 (FOXA2, specifically expressed in GE) regulates leukaemia inhibitory factor (LIF) expression (a GE-derived factor expressed transiently on GD 4 [44]) induced by estrogen and progesterone via the corresponding estrogen receptor α (ESRα) and progesterone receptor (PGR) for blastocyst implantation and the subsequent endometrial decidualization [45–47]. FOXA2 showed significantly higher expression in the HA/ABs group (white arrows in Fig. 4a) than in the other three groups (Fig. 4a, c). The total PGR expression in endometrium was similar across the four groups (Fig. S7a); ESRα was more abundant in the epithelium of the HA/ABs group (white arrows in Fig. 4a) than in that of the other three groups (Fig. 4a, d), consistent with the total ESRα expression in endometrium in the four groups (Fig. S7b). Higher LIF expression in the epithelium (white arrows in Fig. 4a) of the HA/ABs group was observed than in that of the NR, ABs, and HA groups (Fig. 4a, e), consistent with the total LIF expression in endometrium in the four groups (Fig. S7c).

3.7. Cell-free AB-laden HA hydrogel promotes fertility restoration in the murine endometrial damage model

Pregnancy rates were significantly higher in the HA/ABs group than in the NR and ABs groups (Table 1). The number of growing embryos in each uterine horn in the HA/ABs group was significantly higher than that in the NR group (Fig. 4f). Observation of pregnant mice from the HA/ABs groups between GD 6 and 19 demonstrated continuous development through the course of pregnancy (Fig. 4g), and on GD 19, the embryos and placenta were normal in size (Fig. 4h). H&E staining

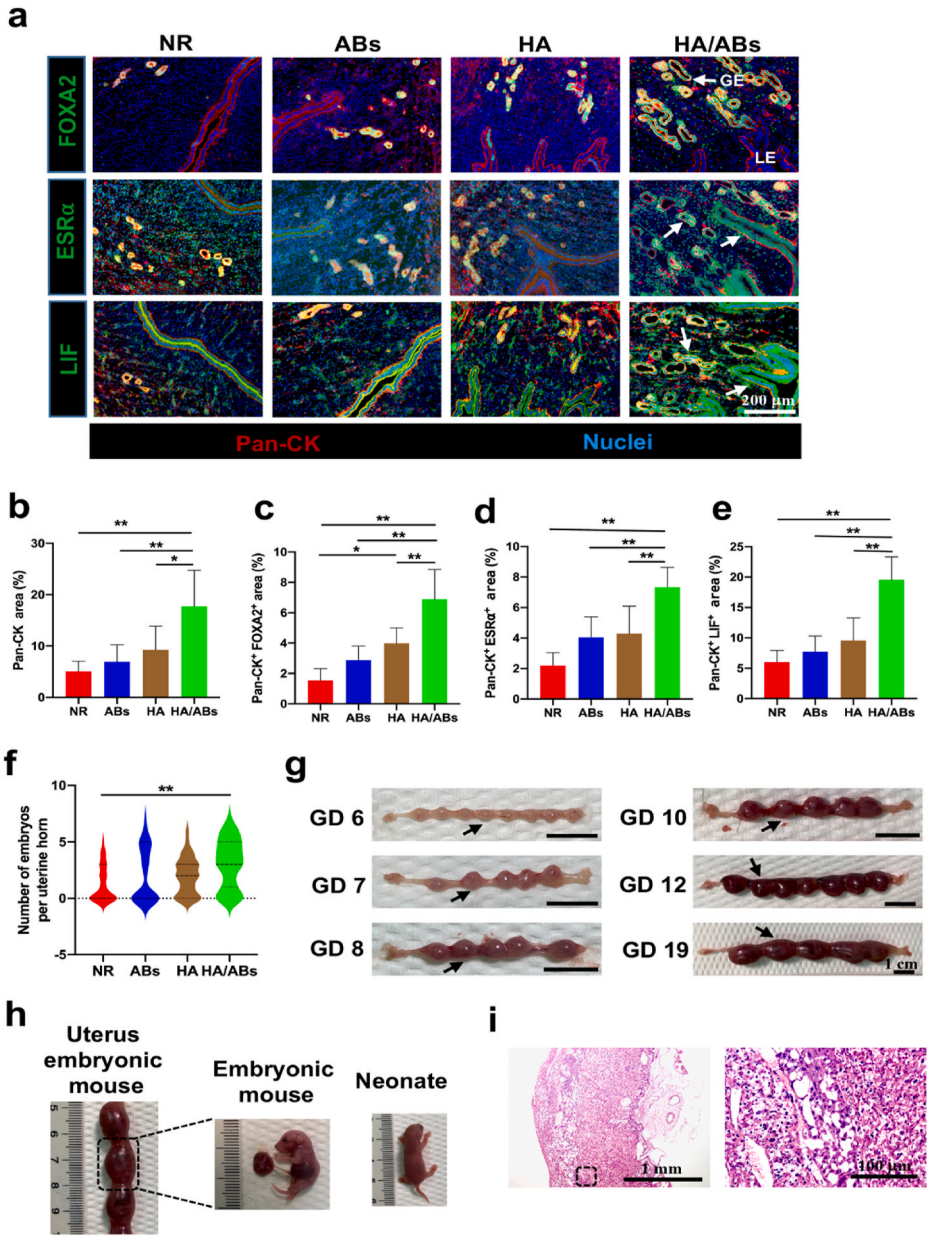

Fig. 4. Endometrial receptivity refunction and fertility restoration induced by the AB-laden HA hydrogel in the murine acute endometrial damage model. (Print in color) a) Representative images of immunofluorescence staining for FOXA2 (green), ESRα (green), and LIF (green) in the endometrium on gestational day (GD) 4. The endometrium was counterstained with anti-pan-cytokeratin antibody (Pan-CK, red) to visualize the epithelium and DAPI (blue) to visualize the nuclei. GE, glandular epithelium; LE, luminal epithelium. Positive staining for FOXA2, ESRα, and LIF in the epithelium in the HA/ABs group are indicated by white arrows. Quantification of the Pan-CK$^+$ area (b), the Pan-CK$^+$ and FOXA2$^+$ area (c), the Pan-CK$^+$ and ESR-α$^+$ area (d) and the Pan-CK$^+$ and LIF$^+$ area (e) in the endometrium on GD 4 (n = 6). f) Violin plots showing the number of growing embryos per uterine horn following treatment (n = 31 in the NR and ABs groups, n = 33 in the HA and HA/ABs groups). g) Gross morphology of uterine horns from the HA/ABs group on GD 6, 7, 8, 10, 12, and 19. Black arrowheads indicate individual implantation sites. h) Mouse embryos and neonates from the HA/ABs group. i) Representative images of the placenta from the HA/ABs group on GD 19, examined using hematoxylin and eosin staining. The insets outlined by black dashed boxes are shown at a higher magnification. NR, natural repair without any treatment; ABs, injection of an AB solution only; HA, injection of HA only; HA/ABs, injection of the AB-laden HA hydrogel. *$p < 0.05$ and **$p < 0.01$.

Table 1
Reproductive outcomes 12 days following the different treatments in the murine endometrial damage model.

Treatment	Number of uterine horns with growing embryos	Total number of uterine horns	Rate of pregnancy (%)
NR	15	31	48.4[a,b]
ABs	15	31	48.4[c,d]
HA	24	33	72.7
HA/ABs	26	33	78.8

NR, natural repair without any treatment; ABs, injection of the AB solution only; HA, injection of HA only; HA/ABs, injection of the AB-laden HA hydrogel.
[a] $p < 0.05$ NR versus HA.
[b] $p < 0.01$ NR versus HA/ABs.
[c] $p < 0.05$ ABs versus HA.
[d] $p < 0.01$ ABs versus HA/ABs.

showed that the placenta in the HA/ABs group was highly vascularized in structure (Fig. 4i). Finally, mice in the HA/ABs group were found to have given birth to normal-looking neonates (Fig. 4h).

3.8. Mechanism underlying the endometrial regeneration induced by the AB-laden HA hydrogel in vivo

Macrophages have been reported to play a critical role in tissue regeneration, and different macrophage types show spatiotemporal changes after tissue injury to adapt to the requirements of tissue regeneration [48]. A higher infiltration of macrophages (assessed by F4/80) was observed in the ABs and HA/ABs groups at 3 d post-surgery than in the NR and HA groups, with maximal staining observed in the HA/ABs group at 7 d post-surgery (Fig. 5a, Fig. S8a). Concurrent with the F4/80 expression, CD163 and CD86 expression in the ABs group and HA/ABs groups was also higher at 3 d post-operation than that in the NR and HA groups, with maximal staining observed in the HA/ABs group at 7 d post-surgery (Fig. 5b, c, Fig. S8b). Then we measured the fraction of both $CD163^+$ and $CD86^+$ cells (Fig. 5d). Interestingly, the cells concurrent expression of CD163 and CD86 were high in the HA/ABs group both at 3 d and 7 d post-surgery. Those results indicated that some of the macrophages were taking on resolution toward M2 macrophage in the HA/ABs group. To confirm the enhanced immunomodulatory effect of AB-laden HA furtherly, we measured cytokines in uterine samples using ELISA analysis (Fig. 5e–h). Among the proinflammatory cytokines, the concentration of IL-6 was reduced at 7 d post-surgery in HA/ABs group, compared with NR and HA groups (Fig. 5e); the concentration of TNF-α is reduced in the HA/ABs group both at 3 d and 7 d post-surgery, compared with HA group (Fig. 5f); the concentration of IL-1β is reduced in the HA/ABs group at 7 d post-surgery, compared with NR and ABs group (Fig. 5g). To be noticed, the HA group exhibited a higher TNF-α expression, and higher concentration of IL-1β was observed in HA and HA/ABs group at 3 d post-surgery, which might attribute to the neutrophil extracellular trap formation surrounding the hydrogel and further activation of inflammatory response [49]. Importantly, the HA/ABs group displayed enhanced concentration of IL-10, which is a critical anti-inflammatory and pro-healing cytokine (Fig. 5h).

The number of $Ki67^+$ (marker of proliferative cell) cells was significantly higher in the ABs and HA/ABs groups at 3 d post-surgery than in

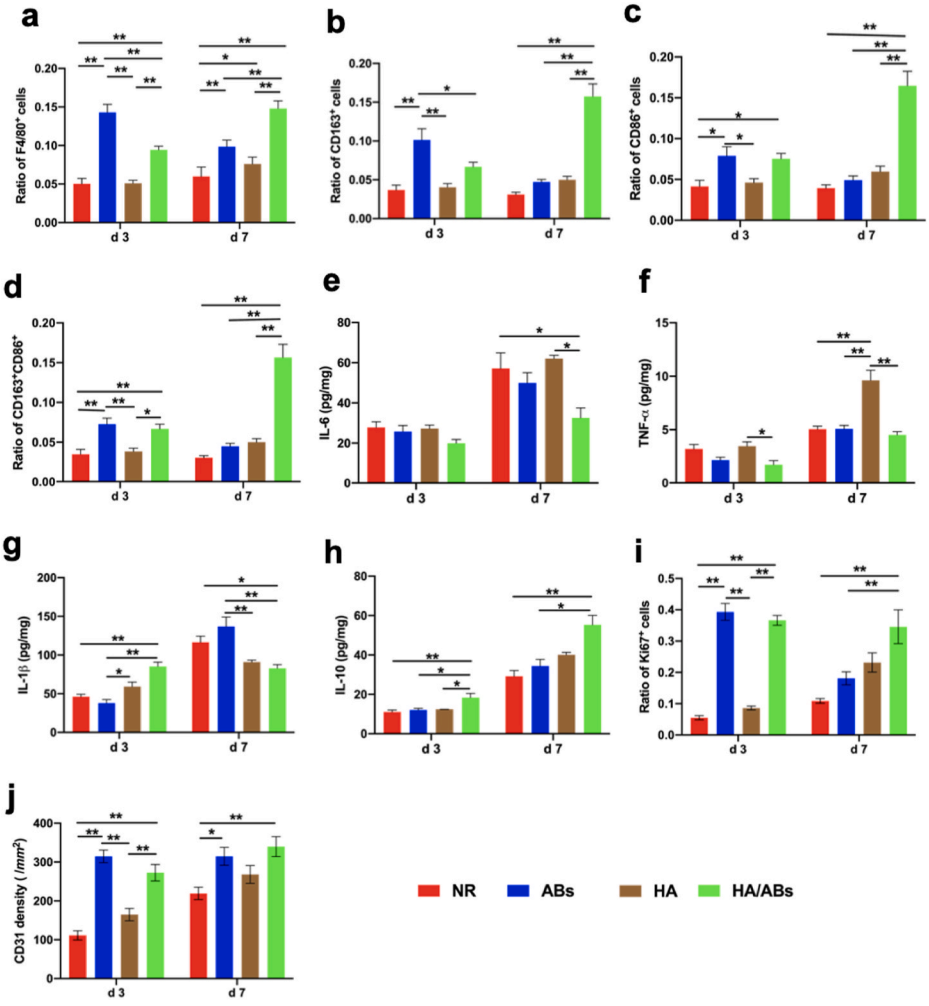

Fig. 5. Macrophage immunomodulation, cell proliferation, and neovascularization induced by the AB-laden HA hydrogel in the murine acute endometrial damage model. (Print in colour) Statistical analysis was performed to examine the expressions of F4/80 (a) (marker of macrophages), CD163 (b) (marker of M2 macrophages), CD86 (c) (marker of M1 macrophages) and concurrent expression of CD163 and CD86 (d) (n = 8). ELISA for IL-6 (e), TNF-α (f), IL-1β (g) and IL-10 (h) in uteri under different treatments (n = 4). Statistical analysis was performed to examine the expressions of Ki67 (e) (marker associated with cell proliferation) and CD31 (f) (marker of capillary vessels) (n = 8). The results in a-d, i and j were normalized to the total number of cells per view under a 400 × magnification and expressed as a ratio of the total number of cells positive for a marker to the total number of cells present. NR, natural repair without any treatment; ABs, injection of an AB solution only; HA, injection of HA only; HA/ABs, injection of the AB-laden HA hydrogel. *$p < 0.05$ and **$p < 0.01$.

the NR and HA groups, with maximal staining observed in the HA/ABs group at 7 d post-surgery (Fig. 5i, Fig. S8c). There was no difference between ABs group and HA/ABs group at 3 d post-surgery and the proliferating cells was significantly higher in the HA/ABs group at 7 d post-surgery than in the ABs group. It seemed that ABs directly injection could induce active function at the early stage following surgery. However, the therapeutic function was insufficient at the late stage — the AB solution flew out of the uterine cavity, resulting in the low retention of ABs in the wounded area.

Given that angiogenesis is important for the fine restoration of endometrial structure because it is required for oxygen and nutrient delivery [50], we assessed neovascularization using CD31 immunostaining. Increased CD31 staining was observed in the ABs and HA/ABs groups at 3 and 7 d post-surgery relative to the NR and HA groups (Fig. 5j, Fig. S8d). There was no difference between ABs group and HA/ABs group both at 3 d and 7 d post-surgery, which indicated that the administration of ABs only could induce effective angiogenesis. In addition, the HA group exhibited a trend of increased expression of Ki 67^+ cells and $CD31^+$ cells compared with the NR group, although there was no statistical significance. The only HA hydrogel strategy was insufficient, which might attribute to the relatively rapid degradation of HA.

3.9. Cell-free AB-laden HA hydrogel therapy in a rat IUA model

A rat IUA model was used as a translational tool in endometrial research because the fibrosis after severe endometrial damage in the IUA model is similar to the histopathological changes of severe IUA in humans. The IUA model was confirmed to have a thinner endometrium, fewer glands, and increased collagen deposition than normal endometrium (Figs. S9a, b, c). As schematic shown in Fig. 6a, repair outcomes were assessed at days 30 and 60; fertility restoration was assessed at GD 14–19. Treatment with the AB-laden HA hydrogel resulted in a relatively normal appearance of uterine horns (Fig. S9d) and increased endometrial thickness (Fig. 6b, c, Fig. S9e) and numbers of endometrial glands (Fig. 6b, d, Fig. S9e) at both days 30 and 60. Endometrial fibrosis at days 30 and 60 was lower in the HA/ABs group than in the NR, HA, and ABs groups (Fig. 6b, e, Fig. S9e). More importantly, the HA/ABs group showed the highest rate of pregnancy (Table 2), and the number of growing embryos in each uterine horn was significantly higher in the HA/ABs group than in the NR and HA groups (Fig. 6f). On GD 19, the placenta, embryos, and neonates from the HA/ABs group appeared

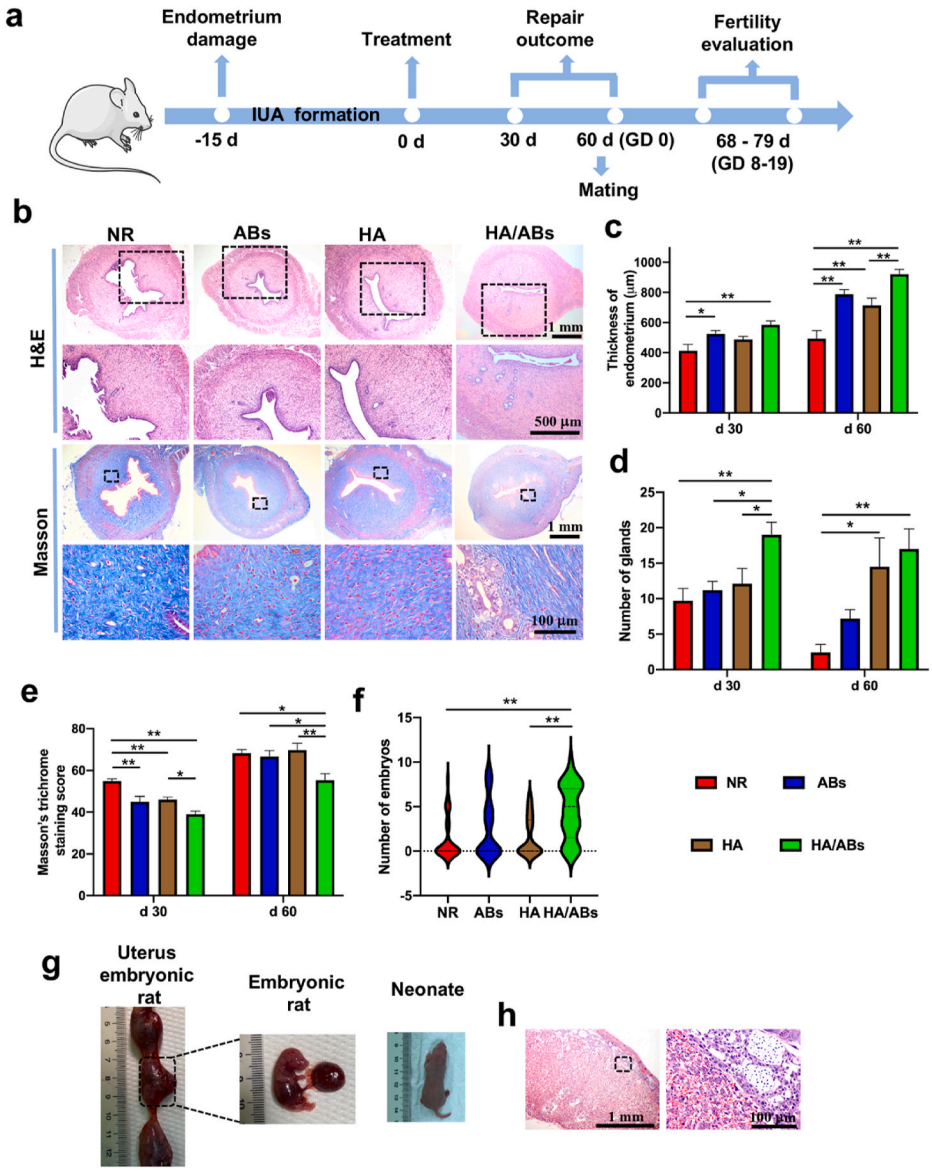

Fig. 6. Endometrial regeneration, collagen remodeling, and fertility restoration induced by the AB-laden HA hydrogel in a rat intrauterine adhesion model. (Print in colour) a) Schematic of the *in vivo* animal experiment procedure. b) Representative images of uteri treated for 60 d, examined using hematoxylin and eosin (H&E) staining and Masson's trichrome staining. The insets outlined by black dashed boxes are shown in the lower row at a higher magnification. c) Quantification of endometrial thickness at days 30 and 60 post-surgery using H&E staining (n = 10). d) Quantification of endometrial glands at days 30 and 60 post-surgery using H&E staining (n = 10). e) Masson's trichrome staining scores for uteri at days 30 and 60 after treatment (n = 10). f) Violin plots showing the number of embryos per uterine horn following different treatments (n = 33 in the NR and ABs groups, n = 29 in the HA and HA/ABs groups). g) Rat embryos at gestational day (GD) 19 and neonate from the HA/ABs group. h) Representative images of placenta from the HA/ABs group obtained on GD 19 examined using H&E staining. The insets outlined by black dashed boxes are shown at a higher magnification. *p < 0.05 and **p < 0.01. NR, natural repair after synechiae division; ABs, injection of an AB solution only after synechiae division; HA, injection of HA only after synechiae division; HA/ABs, injection of the AB-laden HA hydrogel after synechiae division.

Table 2
Reproductive outcomes 60 days following the different treatments in the rat intrauterine adhesion model.

Treatment	Number of uterine horns with growing embryos	Total number of uterine horns	Rate of pregnancy (%)
NR	10	33	30.3 [a]
ABs	15	33	45.5[b]
HA	12	29	41.4[c]
HA/ABs	23	29	79.3

NR, natural repair after synechiae division; ABs, injection of the AB solution only after synechiae division; HA, injection of HA only after synechiae division; HA/ABs, injection of the AB-laden HA hydrogel after synechiae division.
[a] $p < 0.01$ NR versus HA/ABs.
[b] $p < 0.05$ ABs versus HA/ABs.
[c] $p < 0.01$ HA versus HA/ABs.

normal (Fig. 6g). H&E staining also confirmed the highly vascularized structure of the placenta in the HA/ABs group (Fig. 6h).

4. Discussion

Evidence shows that most implanted cells undergo apoptosis after grafting [51,52]. It is speculated that as apoptotic MSCs remain alive for a short period after grafting, they could release soluble factors that could diffuse within the tissue and influence neighboring cells. To date, only a few studies have reported any wound-healing effects of ABs derived from living cells [25–27]. The feasibility of using ABs derived from stem cells for endometrial repair, as an alternative to living cell-based therapy, has not been explored.

In the present study, in one treatment, ABs were directly injected into the uterine cavity, which led to indistinct therapeutic results, and this delivery strategy was obviously insufficient — the AB solution flew out of the uterine cavity, resulting in the low retention of ABs in the wounded area. Here, we embedded ABs within a HA hydrogel to generate a fully acellular scaffold and the composite hydrogel used a "vesicles in matrix" design: The ABs exerted therapeutic effects, whereas the HA promoted the retention of ABs at the site of interest while acting as a separator that aids in preventing adhesion in the uterine cavity. Meanwhile, the suitable viscosity of HA hydrogels makes it feasible to administer them to the irregular uterine cavity via a minimally invasive injection. Notably, the porous structure of HA permits ABs to be well incorporated and entrapped, making this matrix an adequate carrier for ABs. Further, the kinetics of AB release from HA seem to be suitable for the process of rodent endometrial repair.

We explored the potential mechanism of ABs function *in vitro* and action of the AB-laden HA hydrogel in a murine model of acute endometrial damage within 7 days post-surgery. Macrophage is vital for tissue repair and homeostasis. Macrophage depletion resulted in failure tissue repair in many animal models, while the supplementation or recruitment of macrophages could successfully promote regeneration [49,53]. Particularly, M2 macrophage has been proved to facilitate the resolution of inflammation and healing of wounded tissue by IL-10 [49]. In the study *in vitro*, ABs successfully induced macrophage polarization to the M2 phenotype, and inhibited the expression of genes associated with inflammatory reactions (*IL-1β*, *TNFα*, *IL-6*, and *IFN-γ*), while simultaneously enhancing expression of neovascularization related markers (*VEGFA* and *IGF1*). Even in LPS-primed macrophages, AB treatment effectively induced the expression of pro-healing genes (*IL-10*, *VEGFA*, *IGF1*, and *TGFβ*). In the study *in vivo*, the AB-laden HA hydrogel provided enhanced macrophage recruitment and increased numbers of M2 macrophages, along with the high level of IL-10. Based on these results, MSC-derived ABs exert extensive immunomodulation effect on macrophages, which contributes to macrophage polarization towards the pro-healing phenotype in IUA treatment. In addition, the cells proliferation and neovascularization were accelerated by AB treatment *in vitro* and the effect was strengthened by AB-laden HA implantation *in vivo*. All these active effects of ABs were associated to the enhancement of recipient cells' mitochondrial bioenergetics. lncRNA in ABs might give the remarkable effects through the activation of mitochondrial bioenergetics and additional experiments are required so as to decipher the specific functions of enriched lncRNAs.

The efficacy of the AB-laden HA hydrogel was confirmed in the murine model of acute endometrial damage firstly. The injection of the AB-laden HA hydrogel increased endometrial thickness and the number of endometrial glands, decreased the area of fibrosis, improved endometrial receptivity, and finally promoted fertility restoration. IUA is caused by trauma to the basal layer of the endometrium, always resulting in severe fibrosis that obliterate the uterine cavity. Apparently, Etiological and pathological changes in the model of murine acute endometrial damage are obviously different from clinical intrauterine adhesions. To evaluate the effect of the AB-laden HA in a model of IUAs that more closely resembles that of humans, a further evaluation of the AB-laden HA on a rat model of IUA was performed and the AB-laden HA on IUA therapy was evidenced furtherly.

To be noted, the HA hydrogel injection also led to a higher pregnant rate compared to the ABs group and NR group, likely owing to the separation effect and capacity to activate the endogenous stem cells of HA hydrogel at the site of injury [54]. However, capacity for fine structure restoration and embryos growing was still limited by HA hydrogel from result *in vivo*, which indicated the treatment of HA hydrogel only was inadequate. Interestingly, our previous studies demonstrated an increased rate of pregnancy (40.6%) following the implantation of a huMSC-derived exosomes/collagen scaffold (100 μl 3×10^{11}/mL exosomes derived from 2×10^7 cells) in a rat endometrial damage model [32]. In present study, the rate of pregnancy was furtherly increased (78.8% in the murine endometrium damage model and 79.3% in the rat IUA model) after AB-laden HA hydrogen injection (96 μg ABs derived from 6×10^6 cells). Less huMSCs were needed for AB isolation and higher pregnancy rate was obtained after the AB-laden HA hydrogel implantation, compare with exosome-based therapy. Besides these therapeutic advantages, there are also some technical advantages of ABs, although there was probably no significant difference in the use of ABs and exosomes. First, the biogenesis of cell apoptosis is more extensive understanding than that of exosomes. Better understanding facilitated controllable manufacturing process via standard operating procedures. Second, the efficiency of MSCs secreting ABs is much higher than that of secreting exosomes, as cytoplastic contents and cell membrane are enveloped into vesicles during the apoptosis process. It is indicated that the entrapment efficiency of active components into ABs should be quite high and comparable to that into exosomes. Additionally, by RNA-seq analysis from ABs, ABs contained a multitude of miRNAs, mRNAs and lncRNAs, which were bioactive and confer the overall functional benefits as an ensemble.

There are some limitations to the study that must be acknowledged. First, whether ABs induced by acute UV exposure carried toxic components is unclear. However, no tumorigenesis occurred during the process of endometrial repair and following pregnancy in the rodent model; the proinflammatory cytokines (IL-6, TNF-α, IL-1β) were not enhanced after ABs uterine cavity injection. Importantly, ABs could exert macrophage phenotype immunomodulation by suppressing the expression of proinflammatory cytokines evidenced *in vivo* and *in vitro*. Nevertheless, because of the known increasing risks of skin cancer by chronic UV exposure [55], more security assessments should be performed on ABs in the future study, especially in the reproductive organs. Second, although the observations from our rodent studies were sufficiently powered, future studies among macaques involving a sufficient sample size and follow-up duration are necessary before clinical translation. In conclusion, the acellular AB-laden HA hydrogel overcomes the limitations of live cell transplantation and provides a novel and promising strategy for endometrial regeneration in cases of IUAs.

5. Conclusions

We proved that the ABs showed positive effects on macrophage immunomodulation, cell proliferation, and angiogenesis via an increase in the mitochondrial bioenergetics of recipient cells *in vitro*. By integrating ABs with a HA hydrogel, we developed an AB delivery system in which HA promoted AB retention and facilitated their continuous release. The implantation of the AB-laden HA hydrogel increased the thickness of the endometrium and the number of endometrial glands, reduced fibrosis, and also promoted endometrial receptivity and fertility restoration in a murine model of acute endometrial damage. The efficacy of the AB-laden HA hydrogel was further confirmed in a rat model of intractable IUA. The *in vivo* mechanism of the AB-laden HA hydrogel implantation was associated with macrophage immunomodulation, cell proliferation, and neovascularization, consistent with the *in vitro* findings. Hence, our study proved the therapeutic potentials of AB and the AB-laden HA hydrogel displayed a clinically feasible and novel therapy for endometrial regeneration and IUA treatment.

CRediT authorship contribution statement

Liaobing Xin: Conceptualization, Data curation, Formal analysis, Funding acquisition, Investigation, Methodology, Project administration, Validation, Writing – original draft, Writing – review & editing. **Cheng Wei:** Conceptualization, Data curation, Formal analysis, Investigation, Methodology, Project administration, Validation, Writing – review & editing. **Xiaomei Tong:** Conceptualization, Data curation, Investigation, Methodology, Project administration, Validation, Writing – review & editing. **Yangyang Dai:** Investigation, Methodology, Project administration, Validation, Writing – review & editing. **Dong Huang:** Conceptualization, Writing – review & editing. **Jianmin Chen:** Conceptualization, Writing – review & editing. **Lie Ma:** Conceptualization, Funding acquisition, Project administration, Resources, Supervision, Writing – review & editing. **Songying Zhang:** Conceptualization, Funding acquisition, Project administration, Resources, Supervision, Writing – review & editing.

Declaration of competing interest

The authors declare that they have no known competing financial interests or personal relationships that could have appeared to influence the work reported in this paper.

Acknowledgements

The authors thank the funding support by the National Key Research Program of China (2018YFC1004800), the International (Regional) Cooperation and Exchange Program of China (82061160494), the National Natural Science Foundation of China (51873184) and the Fundamental Research Funds for the Central Universities (2021FZZX005-16).

Appendix A. Supplementary data

Supplementary data to this article can be found online at https://doi.org/10.1016/j.bioactmat.2021.10.025.

References

[1] R. Rai, L. Regan, Recurrent miscarriage, Lancet 368 (2006) 601–611, https://doi.org/10.1016/S0140-6736(06)69204-0.
[2] A.B. Hooker, R.A. de Leeuw, P.M. van de Ven, H.A.M. Brölmann, J.A.F. Huirne, Reproductive performance of women with and without intrauterine adhesions following recurrent dilatation and curettage for miscarriage: long-term follow-up of a randomized controlled trial, Hum. Reprod. 36 (2021) 70–81, https://doi.org/10.1093/humrep/deaa289.
[3] A.R. Gilman, K.M. Dewar, S.A. Rhone, M.R. Fluker, Intrauterine adhesions following miscarriage: look and learn, J. Obstet. Gynaecol. Can. 38 (2016) 453–457, https://doi.org/10.1016/j.jogc.2016.03.003.
[4] A.B. Hooker, M. Lemmers, A.L. Thurkow, M.W. Heymans, B.C. Opemeer, H.A. M. Brölmann, B.W. Mol, J.A.F. Huirne, Systematic review and meta-analysis of intrauterine adhesions after miscarriage: prevalence, risk factors and long-term reproductive outcome, Hum. Reprod. Update 20 (2014) 262–278, https://doi.org/10.1093/humupd/dmt045.
[5] E. Dreisler, J.J. Kjer, Asherman's syndrome: current perspectives on diagnosis and management, Int. J. Womens Health 11 (2019) 191–198, https://doi.org/10.2147/IJWH.S165474.
[6] X. Lin, F. Zhou, M. Wei, Y. Yang, Y. Li, T.C. Li, S. Zhang, Randomized, controlled trial comparing the efficacy of intrauterine balloon and intrauterine contraceptive device in the prevention of adhesion reformation after hysteroscopic adhesiolysis, Fertil. Steril. 104 (2015) 235–240, https://doi.org/10.1016/j.fertnstert.2015.04.008.
[7] X. Yang, Y. Liu, T.C. Li, E. Xia, Y. Xiao, F. Zhou, D. Song, Q. Zhou, Durations of intrauterine balloon therapy and adhesion reformation after hysteroscopic adhesiolysis: a randomized controlled trial, Reprod. Biomed. Online 40 (2019) 539–546, https://doi.org/10.1016/j.rbmo.2019.11.017.
[8] Y. Chi, P. He, L. Lei, Y. Lan, J. Hu, Y. Meng, L. Hu, Transdermal estrogen gel and oral aspirin combination therapy improves fertility prognosis via the promotion of endometrial receptivity in moderate to severe intrauterine adhesion, Mol. Med. Rep. 17 (2018) 6337–6344, https://doi.org/10.3892/mmr.2018.8685.
[9] X. Shi, S.H. Saravelos, Q. Zhou, X. Huang, E. Xia, Prevention of postoperative adhesion reformation by intermittent intrauterine balloon therapy: a randomised controlled trial, BJOG 126 (2019) 1259–1266, https://doi.org/10.1111/1471-0528.15843.
[10] X. Mao, Y. Tao, R. Cai, J. Zhang, H. Gao, Q. Chen, Y. Kuang, S. Zhang, Cross-linked hyaluronan gel to improve pregnancy rate of women patients with moderate to severe intrauterine adhesion treated with IVF: a randomized controlled trial, Arch. Gynecol. Obstet. 301 (2020) 199–205, https://doi.org/10.1007/s00404-019-05368-6.
[11] Y. Cao, H. Sun, H. Zhu, X. Zhu, X. Tang, G. Yan, J. Wang, D. Bai, J. Wang, L. Wang, Q. Zhou, H. Wang, C. Dai, L. Ding, B. Xu, Y. Zhou, J. Hao, J. Dai, Y. Hu, Allogeneic cell therapy using umbilical cord MSCs on collagen scaffolds for patients with recurrent uterine adhesion: a phase I clinical trial, Stem Cell Res. Ther. 9 (2018) 192, https://doi.org/10.1186/s13287-018-0904-3.
[12] X. Santamaria, S. Cabanillas, I. Cervello, C. Arbona, F. Raga, J. Ferro, J. Palmero, J. Remohi, A. Pellicer, C. Simon, Autologous cell therapy with CD133+ bone marrow-derived stem cells for refractory Asherman's syndrome and endometrial atrophy: a pilot cohort study, Hum. Reprod. 31 (2016) 1087–1096, https://doi.org/10.1093/humrep/dew042.
[13] J. Tan, P. Li, Q. Wang, Y. Li, X. Li, D. Zhao, X. Xu, L. Kong, Autologous menstrual blood-derived stromal cells transplantation for severe Asherman's syndrome, Hum. Reprod. 31 (2016) 2723–2729, https://doi.org/10.1093/humrep/dew235.
[14] Z. Guo, X. Sun, X. Xu, Q. Zhao, J. Peng, Y. Wang, Human umbilical cord mesenchymal stem cells promote peripheral nerve repair via paracrine mechanisms, Neural, Regen. Res. 10 (2015) 651–658, https://doi.org/10.4103/1673-5374.155442.
[15] J. Li, Q. Mao, J. He, H. She, Z. Zhang, C. Yin, Human umbilical cord mesenchymal stem cells improve the reserve function of perimenopausal ovary via a paracrine mechanism, Stem Cell Res. Ther. 8 (2017) 55, https://doi.org/10.1186/s13287-017-0514-5.
[16] J.A. Heslop, T.G. Hammond, I. Santeramo, A.T. Piella, I. Hopp, J. Zhou, R. Baty, E. I. Graziano, B.P. Marco, A. Caron, P. Skold, P.W. Andrews, M.A. Baxter, D.C. Hay, J. Hamdam, M.E. Sharpe, S. Patel, D.R. Jones, J. Reinhardt, E.H.J. Danen, U. Ben-David, G. Stacey, P. Bjorquist, J. Piner, J. Mills, C. Rowe, G. Pellegrini, S. Sethu, D. J. Antoine, M.J. Cross, P. Murray, D.P. Williams, N.R. Kitteringham, C.E. P. Goldring, B.K. Park, Concise review: workshop review: understanding and assessing the risks of stem cell-based therapies, Stem Cells Transl. Med. 4 (2015) 389–400, https://doi.org/10.5966/sctm.2014-0110.
[17] A.K.A. Silva, S. Perretta, G. Perrod, L. Pidial, V. Lindner, F. Carn, S. Lemieux, D. Alloyeau, I. Boucenna, P. Menasché, B. Dallemagne, F. gazeau, C. Wilhelm, C. Cellier, O. Clément, G. Rahmi, Thermoresponsive gel embedding with adipose stem cell-derived extracellular vesicles promotes esophageal fistula healing in a thermo-actuated delivery strategy, ACS Nano 12 (2018) 9800–9814, https://doi.org/10.1021/acsnano.8b00117.
[18] B. Liu, B.W. Lee, K. Nakanishi, A. Villasante, R. Williamson, J. Metz, J. Kim, M. Kanai, L. Bi, K. Brown, G.D. Paolo, S. Homma, P.A. Sims, V.K. Topkara, G. Vunjak-Novakovic, Cardiac recovery via extended cell-free delivery of extracellular vesicles secreted by cardiomyocytes derived from induced pluripotent stem cells, Nat. Biomed. Eng. 2 (2018) 293–303, https://doi.org/10.1038/s41551-018-0229-7.
[19] M.Á. Brennan, P. Layrolle, D.J. Mooney, Biomaterials functionalized with MSC secreted extracellular vesicles and soluble factors for tissue regeneration, Adv. Funct. Mater. 30 (2020), 1909125, https://doi.org/10.1002/adfm.201909125.
[20] J. Fan, C. Lee, S. Kim, C. Chen, T. Aghaloo, M. Lee, Generation of small RNA-modulated exosome mimetics for bone regeneration, ACS Nano 14 (2020) 11973–11984, https://doi.org/10.1021/acsnano.0c05122.
[21] X. Xu, Y. Lai, Z. Hua, Apoptosis and apoptotic body: disease message and therapeutic target potentials, Biosci. Rep. 39 (2019), BSR20180992, https://doi.org/10.1042/BSR20180992.
[22] H.D. Ryoo, T. Gorenc, H. Steller, Apoptotic cells can induce compensatory cell proliferation through the JNK and the Wingless signaling pathways, Dev. Cell 7 (2004) 491–501, https://doi.org/10.1016/j.devcel.2004.08.019.

[23] C.K. Brock, S.T. Wallin, O.E. Ruiz, K.M. Samms, A. Mandal, E.A. Sumner, G. T. Eisenhoffer, Stem cell proliferation is induced by apoptotic bodies from dying cells during epithelial tissue maintenance, Nat. Commun. 10 (2019) 1044, https://doi.org/10.1038/s41467-019-09010-6.
[24] C.B. Medina, P. Mehrotra, S. Arandjelovic, J.S.A. Perry, Y. Guo, S. Morioka, B. Barron, S.F. Walk, B. Ghesquiere, A.S. Krupnick, U. Lorenz, K.S. Ravichandran, Metabolites released from apoptotic cells act as tissue messengers, Nature 580 (2020) 130–135, https://doi.org/10.1038/s41586-020-2121-3.
[25] D. Liu, X. Kou, C. Chen, S. Liu, Y. Liu, W. Yu, T. Yu, R. Yang, R. Wang, Y. Zhou, S. Shi, Circulating apoptotic bodies maintain mesenchymal stem cell homeostasis and ameliorate osteopenia via transferring multiple cellular factors, Cell Res. 28 (2018) 918–933, https://doi.org/10.1038/s41422-018-0070-2.
[26] J. Liu, X. Qiu, Y. Lv, C. Zheng, Y. Dong, G. Dou, B. Zhu, A. Liu, W. Wang, J. Zhou, S. Liu, S. Liu, B. Gao, Y. Jin, Apoptotic bodies derived from mesenchymal stem cells promote cutaneous wound healing via regulating the functions of macrophages, Stem Cell Res. Ther. 11 (2020) 507, https://doi.org/10.1186/s13287-020-02014-w.
[27] Q. Ma, M. Liang, N. Limjunyawong, Y. Dan, J. Xing, J. Li, J. Xu, C. Dou, Osteoclast-derived apoptotic bodies show extended biological effects of parental cell in promoting bone defect healing, Theranostics 10 (2020) 6825–6838, https://doi.org/10.7150/thno.45170.
[28] L. Ding, X. Li, H. Sun, J. Su, N. Lin, B. Peault, T. Song, J. Yang, J. Dai, Y. Hu, Transplantation of bone marrow mesenchymal stem cells on collagen scaffolds for the functional regeneration of injured rat uterus, Biomaterials 35 (2014) 4888–4900, https://doi.org/10.1016/j.biomaterials.2014.02.046.
[29] Y.Y. Kim, K. Park, Y.J. Kim, M.S. Kim, H.C. Liu, Z. Rosenwaks, S. Ku, Synergistic regenerative effects of functionalized endometrial stromal cells with hyaluronic acid hydrogel in a murine model of uterine damage, Acta Biomater. 89 (2019) 139–151, https://doi.org/10.1016/j.actbio.2019.03.032.
[30] L. Wang, C. Yu, T. Chang, M. Zhang, S. Song, C. Xiong, P. Su, W. Xiang, In situ repair abilities of human umbilical cord-derived mesenchymal stem cells and autocrosslinked hyaluronic acid gel complex in rhesus monkeys with intrauterine adhesion, Sci. Adv. 6 (2020), https://doi.org/10.1126/sciadv.aba6357 eaba6357.
[31] L. Xin, X. Lin, Y. Pan, X. Zheng, L. Shi, Y. Zhang, L. Ma, C. Gao, S. Zhang, A collagen scaffold loaded with human umbilical cord-derived mesenchymal stem cells facilitates endometrial regeneration and restores fertility, Acta Biomater. 92 (2019) 160–171, https://doi.org/10.1016/j.actbio.2019.05.012.
[32] L. Xin, X. Lin, F. Zhou, C. Li, X. Wang, H. Yu, Y. Pan, H. Fei, L. Ma, S. Zhang, A scaffold laden with mesenchymal stem cell-derived exosomes for promoting endometrium regeneration and fertility restoration through macrophage immunomodulation, Acta Biomater. 113 (2020) 252–266, https://doi.org/10.1016/j.actbio.2020.06.029.
[33] H. Tan, C.R. Chu, K.A. Payne, K.G. Marra, Injectable in situ forming biodegradable chitosan-hyaluronic acid based hydrogels for cartilage tissue engineering, Biomaterials 30 (2009) 2499–2506, https://doi.org/10.1016/j.biomaterials.2008.12.080.
[34] J.A. Burdick, G.D. Prestwich, Hyaluronic acid hydrogels for biomedical applications, Adv. Mater. 23 (2011), https://doi.org/10.1002/adma.201003963. H41−56.
[35] Z. Fei, X. Xin, H. Fei, C. Yuechong, Meta-analysis of the use of hyaluronic acid gel to prevent intrauterine adhesions after miscarriage, Eur. J. Obstet. Gynecol. Reprod. Biol. 244 (2020) 1–4, https://doi.org/10.1016/j.ejogrb.2019.10.018.
[36] J. Li, Y. Dai, H. Zhu, Y. Jiang, S. zhang, Endometriotic mesenchymal stem cells significantly promote fibrogenesis in ovarian endometrioma through the Wnt/b-catenin pathway by paracrine production of TGF-b1 and Wnt1, Hum. Reprod. 31 (2016) 1224–1235, https://doi.org/10.1093/humrep/dew058.
[37] C. Gil-Sanchis, I. Cervelló, S. Khurana, A. Faus, C. Verfaillie, C. Simon, Contribution of different bone marrow-derived cell types in endometrial regeneration using an irradiated murine model, Fertil. Steril. 103 (2015) 1596–1605, https://doi.org/10.1016/j.fertnstert.2015.02.030.
[38] Y. Zhang, X. Lin, Y. Dai, X. Hu, H. Zhu, Y. Jiang, S. Zhang, Endometrial stem cells repair injured endometrium and induce angiogenesis via AKT and ERK pathways, Reproduction 152 (2016) 389–402, https://doi.org/10.1530/REP-16-0286.
[39] T. Song, X. Zhao, H. Sun, X. Li, N. Lin, L. Ding, J. Dai, Y. Hu, Regeneration of uterine horns in rats using collagen scaffolds loaded with human embryonic stem cell-derived endometrium-like cells, Tissue Eng. 21 (2015) 352–361, https://doi.org/10.1089/ten.TEA.2014.0052.
[40] S. Kilic, B. Yukse, F. Pinarli, A. Albayrak, B. Boztok, T. Delibasi, Effect of stem cell application on Asherman syndrome, an experimental rat model, J. Assist. Reprod. Genet. 31 (2014) 975–982, https://doi.org/10.1007/s10815-014-0268-2.
[41] X. Wang, C. Wang, W. Gou, X. Xu, Y. Wang, A. Wang, W. Xu, Q. Guo, S. Liu, Q. Lu, H. Meng, M. Yuan, J. Peng, S. Lu, The optimal time to inject bone mesenchymal stem cells for fracture healing in a murine model, Stem Cell Res. Ther. 9 (2018) 272.
[42] F. Alawadhi, H. Du, H. Cakmak, H.S. Taylor, Bone marrow-derived stem cell (BMDSC) transplantation improves fertility in a murine model of asherman's syndrome, PLoS One 9 (2014), e96662, https://doi.org/10.1371/journal.pone.0096662.
[43] A.M. Kelleher, J. Milano-Foster, S.K. Behura, T.E. Spencer, Uterine glands coordinate on-time embryo implantation and impact endometrial decidualization for pregnancy success, Nat. Commun. 9 (2018) 2435, https://doi.org/10.1038/s41467-018-04848-8.
[44] C.L. Stewart, P. Kaspar, L.J. Brunet, H. Bhatt, I. Gadi, F. Kontgen, S.J. Abbondanzo, Blastocyst implantation depends on maternal expression of leukaemia inhibitory factor, Nature 359 (1992) 76–79, https://doi.org/10.1038/359076a0.
[45] A.M. Kelleher, W. Peng, J.K. Pru, C.A. Pru, F.J. DeMayo, T.E. Spencer, Forkhead box a2 (FOXA2) is essential for uterine function and fertility, Proc. Natl. Acad. Sci. U. S. A 114 (2017) E1018–E1026, https://doi.org/10.1073/pnas.1618433114.
[46] P. Dhakal, A.M. Kelleher, S.K. Behura, T.E. Spencer, Sexually dimorphic effects of forkhead box a2 (FOXA2) and uterine glands on decidualization and fetoplacental development, Proc. Natl. Acad. Sci. U. S. A 117 (2020) 23952–23959, https://doi.org/10.1073/pnas.2014272117.
[47] M.J. Large, F.J. DeMayo, The regulation of embryo implantation and endometrial decidualization by progesterone receptor signaling, Mol. Cell. Endocrinol. 358 (2012) 155–165, https://doi.org/10.1016/j.mce.2011.07.027.
[48] Z. Julier, A.J. Park, P.S. Briquez, M.M. Martino, Promoting tissue regeneration by modulating the immune system, Acta Biomater. 53 (2017) 13–28, https://doi.org/10.1016/j.actbio.2017.01.056.
[49] J. Won, Y.S. Lee, J. Park, J. Lee, Y.S. Shin, C. Kim, J.C. Knowles, H. Kim, Hierarchical microchanneled scaffolds modulate multiple tissue-regenerative processes of immune-responses, angiogenesis, and stem cell homing, Biomaterials 227 (2020), 119548, https://doi.org/10.1016/j.biomaterials.2019.119548.
[50] J. Lin, Z. Wang, J. Huang, S. Tang, Q. Saiding, Q. Zhu, W. Cui, Microenvironment-protected exosome-hydrogel for facilitating endometrial regeneration, fertility restoration, and live birth of offspring, Small 17 (2021), e2007235, https://doi.org/10.1002/smll.202007235.
[51] M. Zhang, D. Methot, V. Poppa, Y. Fujio, K. Walsh, C.E. Murry, Cardiomyocyte grafting for cardiac repair: graft cell death and anti-death strategies, J. Mol. Cell. Cardiol. 33 (2001) 907–921, https://doi.org/10.1006/jmcc.2001.1367.
[52] J. Park, B. Kim, J. Han, J. Oh, S. Park, S. Ryu, S. Jung, J. Shin, B.S. Lee, B.H. Hong, D. Choi, B. Kim, Graphene oxide flakes as a cellular adhesive: prevention of reactive oxygen species mediated death of implanted cells for cardiac repair, ACS Nano 9 (2015) 4987–4999, https://doi.org/10.1021/nn507149w.
[53] J.W. Godwin, A.R. Pinto, N.A. Rosenthal, Macrophages are required for adult salamander limb regeneration, Proc. Natl. Acad. Sci. U. S. A. 110 (2013) 9415–9420, https://doi.org/10.1073/pnas.1300290110.
[54] C. Chai, K.W. Leong, Biomaterials approach to expand and direct differentiation of stem cells, Mol. Ther. 15 (2007) 467–480, https://doi.org/10.1038/sj.mt.6300084.
[55] T. Murakami, M. Fujimoto, M. Ohtsuki, H. Nakagawa, Expression profiling of cancer-related genes in human keratinocytes following non-lethal ultraviolet, B irradiation 27 (2001) 121–129, https://doi.org/10.1016/s0923-1811(01)00124-4.